Journal of Catalysis **204,** 272–280 (2001)
doi:10.1006/jcat.2001.3393, available online at http://www.idealibrary.com on IDEAL®

Combined Diffusion, Adsorption, and Reaction Studies of *n*-Hexane Hydroisomerization over Pt/H–Mordenite in an Oscillating Microbalance

S. van Donk, A. Broersma, O. L. J. Gijzeman, J. A. van Bokhoven, J. H. Bitter, and K. P. de Jong[1]

Department of Inorganic Chemistry and Catalysis, Debye Institute, Utrecht University, P.O. Box 80083, 3508 TB Utrecht, The Netherlands

Received January 22, 2001; revised May 4, 2001; accepted August 10, 2001; published online October 25, 2001

Uptake experiments under full catalytic conditions have been performed using a tapered element oscillating microbalance. The effect of acid leaching on the diffusivity and reaction of *n*-hexane in Pt/H–mordenite has been established from these experiments. For acid-leached Pt/H–mordenite the hydroisomerization activity is four times higher than for untreated Pt/H–mordenite. Acid leaching gives rise to an acceleration of the uptake of *n*-hexane under reaction conditions. Analysis of the data implies the faster uptake to be predominantly accounted for by a shorter intracrystalline diffusion path length, as diffusivities are in the same range for both catalysts. The shorter path length results from the mesoporous structure of H-mordenite generated by acid leaching. From the diffusivities, from the path lengths, and by using the Thiele model, it is inferred that the intrinsic rate constant of acid-leached Pt/H–mordenite is twice that of the untreated Pt/H–mordenite. The facilitated transport of reactants and products doubles the effectiveness factor, thus also contributing to the overall activity enhancement for *n*-hexane hydroisomerization after acid leaching.

Key Words: **diffusion; adsorption; hydroisomerization; Pt/H–mordenite; *n*-hexane; oscillating microbalance.**

INTRODUCTION

Zeolites are microporous crystalline structures that are widely applied as adsorbents and solid acid catalysts in petroleum and chemical process industries. Transport through zeolitic micropores occurs by diffusion and often affects or even controls the overall rate of the process (1). Optimization of catalytic and adsorption processes therefore requires knowledge of all phenomena that influence diffusional behavior of molecules in such materials. A number of techniques are available to experimentally determine diffusivities in zeolites, but none of them is suitable for simultaneously monitoring adsorption, diffusion, and reaction. This illustrates the need for the development of an experimental procedure to monitor these phenomena concurrently in one setup. A catalysis setup including a tapered element oscillating microbalance (TEOM) offers the possibility of monitoring adsorption and diffusion in a quantitative way, as has been shown by Chen *et al.* (2). At the same time a TEOM provides the possibility of working under representative catalysis conditions, as the properties of a down-flow fixed-bed reactor are maintained. Here we report a first-of-its-kind study using a TEOM in which adsorption and diffusion are measured under full catalytic conditions for the hydroisomerization of *n*-hexane over Pt/H–mordenite.

Pt/H–mordenite is a highly suitable catalyst for the hydroisomerization of linear alkanes to branched ones, although the limited intracrystalline molecular transport may significantly slow down the catalyst performance (3). To this end, it is generally known that acid leaching of the mordenite structure enhances hydroisomerization activity (3–7). In addition, it has been shown that local destruction of the mordenite crystals by growing large Pt particles inside also results in higher hydroisomerization activity (8). In a study by Tromp *et al.* (9) it was demonstrated that acid leaching leads to dealumination and the creation of mesopores that have recently been visualised by three-dimensional (3D) transmission electron microscopy (TEM) (10). This is accompanied by enhanced catalytic activity for *n*-hexane hydroisomerization. Moreover, the selectivity changed slightly to favor primary products (9). The origin of the increased hydroisomerization rate after acid leaching of the mordenite may, in the case of a diffusion limited reaction, be explained by one or more of the following options: (i) an increase in the intracrystalline diffusion coefficient as a result of a faster molecular transport through the micropores; (ii) a decrease in the intracrystalline pathlength L related to the generation of mesopores, again resulting in a faster transport; and/or (iii) an increase in the intrinsic activity (i.e., enhancement of the *n*-hexane hydroisomerization rate per Brønsted acid site).

The present work deals with the adsorptive and diffusional behavior of *n*-hexane in untreated as well as acid-leached Pt/H–mordenite and the simultaneous assessment of their influence on the hydroisomerization performance. We report on the determination of diffusivities and intrinsic activities for the same Pt/H–mordenite catalysts that were evaluated by Tromp *et al.* (9). The *n*-hexane uptake

[1] To whom correspondence should be addressed. Fax: 31 30 2511027. E-mail: K.P.deJong@chem.uu.nl.

0021-9517/01 $35.00

curves are measured in a TEOM reactor under full catalytic conditions. The experimental data obtained with the TEOM setup are fitted into an adapted theoretical model to acquire diffusion coefficients. The application of this method is exemplified by performing check experiments in which the conditions for the *n*-hexane uptake are varied.

Based on both diffusivities as well as catalysis results, intrinsic activities are computed and evaluated. In the end it is shown that both a better accessibility of the crystals as well as an increase in intrinsic activity contributes to the observed increase in the hydroisomerization rate after acid leaching.

EXPERIMENTAL

TEOM

Operation of the TEOM (Rupprecht & Pataschnick TEOM 1500 PMA) is based on the relationship between natural frequency (f) of the oscillating tapered element containing the catalyst and its mass (m),

$$m_2 - m_1 = K_0\left[\left(\frac{1}{f_2}\right)^2 - \left(\frac{1}{f_1}\right)^2\right], \qquad [1]$$

where K_0 is the spring constant for the tapered element used in the experiment and the subscripts 1 and 2 refer to the change of mass and frequency with time. One of the major advantages of the design is that it provides a packed catalyst bed through which all the gas is forced to flow, as depicted in Fig. 1. For a detailed description of the TEOM we refer readers to Chen *et al.* (2) and Zhu *et al.* (11).

Samples

The parent mordenite (HMOR-P) has a zeolite crystal size of 0.2×0.4 μm and Si/Al = 6. The acid-leached mordenite (HMOR-L) has a lower bulk aluminum content (i.e., Si/Al = 20). Physicochemical properties of the H-mordenite samples are presented in Table 1. Clearly, acid leaching generates mesopores in the H-mordenite crystals in line with earlier results from electron microscopy (9, 10). The 2 wt% Pt/H–mordenite (Pt/HMOR) catalysts were prepared as described earlier by Tromp *et al.* (9).

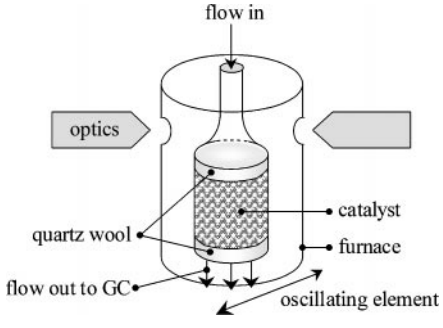

FIG. 1. Schematic picture of the oscillating tapered element with the packed sample bed.

TABLE 1

Physicochemical Characterization of the Mordenite Samples

Sample	HMOR-P	HMOR-L
Mesoporous surface area ($m^2\ g^{-1}$)	30	89
Micropore volume (ml g^{-1})	0.19	0.18
Mesopore volume (ml g^{-1})	0.04	0.11
Si/Al ratio from XRF (mol mol^{-1})	6	20
Acid sites by *n*-propylamine TPD (mmol g^{-1})	2.1	1.1
Acid sites by isopropylamine TPD (mmol g^{-1})	1.4	1.1
Acid sites by ammonia TPD (mmol g^{-1})	2.3	0.7
Pt–Pt coordination number from EXAFS[a]	6.5–7.0	6.5–7.0

[a] Determined for the Pt/HMOR samples.

Experiments

Hydroisomerization of *n*-hexane was carried out in the TEOM reactor so that mass changes occurring during the catalytic action of the Pt/H–mordenite could be monitored *in situ* (i.e., at high temperatures). A back-pressure regulator maintained the pressure of the system at 1.3 bar. Mass flow controllers adjusted the incoming gas flows. The *n*-hexane (Merck) was injected into the system using a high-performance liquid chromatography pump (Shimadzu LC-10AD). The reaction products were analyzed using a Shimadzu 17A gas chromatograph with a GS-GasPro capillary column (fused silica, 15 m × 0.32 mm). The system was heated to avoid condensation of gases.

Prior to testing, the samples were dried and reduced *in situ* in hydrogen at 623 K. Experiments were executed at 523 K and 1.3 bar using ~85 mg of sample with a particle size of 150–425 μm. Adsorption isotherms were determined under transient conditions by varying the *n*-hexane partial pressure at a total pressure of 1.3 bar and a constant H_2 flow. The transient uptake experiments were performed using an *n*-hexane flow of 0.078 mmol min^{-1} and an H_2 flow of 20 ml min^{-1} (H_2 : *n*-C_6 ratio of 11 mol/mol). After the *n*-hexane was added to the feed, $t = 0$ was defined as the last data point before the first mass change detected by the TEOM. All mass changes were corrected for temperature and gas-density differences by performing blank runs over inert samples. In between every experiment, the samples were regenerated in H_2 at 623 K to ensure clean samples. To determine the influence of product formation on the uptake of *n*-hexane, measurements were also performed on samples without Pt. In addition, the *n*-hexane uptake measurements were performed with a lower *n*-hexane partial pressure (H_2 : *n*-C_6 ratio of 22 mol/mol), with a higher flow rate of both *n*-hexane and H_2, and using a lower amount

of catalyst. This allowed testing of whether consistent uptake data could be obtained using the TEOM setup. The reversibility of the adsorption on the samples was checked as well by monitoring the amount of desorbed species following the uptake experiment.

The catalytic conversion of *n*-hexane over the Pt/H–mordenites was determined at steady state adsorption conditions in the TEOM directly following an uptake experiment. Conversion is defined as the ratio of all products ($\neq n$-C_6) to all compounds detected. Selectivities are calculated as the ratio of a certain product to all products ($\neq n$-C_6). To be able to measure all samples at low conversions (<5%), the amount of catalyst and/or the *n*-hexane and H_2 flow were varied (the $H_2 : n$-C_6 ratio was kept constant at 11 mol/mol).

THEORY

Fick's Second Law

The non-steady-state diffusion of *n*-hexane in Pt/H–mordenite is assumed to take place according to Fick's second law, which describes the change in the overall concentration inside the zeolite crystals as a function of time,

$$\frac{\partial C}{\partial t} = D * \left(\frac{\partial^2 C}{\partial x^2}\right), \qquad [2]$$

where x is distance (in meters). However, it contains the inherent assumption that all molecules equally contribute to the process of stochastic displacement. For uptake measurements over zeolites this is usually not true, as molecules inside the zeolite crystals are present in two phases, a mobile phase and an immobile adsorbed phase. Hence, the diffusivity (D) in Eq. [2] corresponds to the uptake diffusivity based on the total concentration inside the zeolite crystals (i.e., including mobile as well as immobile species). To represent diffusivity merely for the mobile species in the zeolite, one has to multiply the measured uptake diffusivity (D_{uptake}) with the ratio of all sorbed species at equilibrium (C_{eq}) and mobile species at equilibrium, resulting in an intrinsic diffusivity (12). In catalysis the diffusion process under steady state conditions is particularly relevant. Therefore, we take the concentration of mobile species to be equal to the concentration in the gas phase (C_{gas}), since kinetic data are also based on the applied gas-phase concentration. The following relation allows then the calculation of the intracrystalline steady state diffusivity (D_{ss}):

$$D_{ss} = \frac{C_{eq}}{C_{gas}} * D_{uptake}. \qquad [3]$$

As the steady state diffusivity is based on the gas-phase concentration of the system, evaluation of diffusion and catalysis results may now be performed using the same concentration basis, which is of major importance, as was stressed by Post (13). Moreover, Garcia and Weisz (12) showed that possible deviations introduced by this assumption are small, even in the nonlinear region of a Langmuir-type adsorption. In general, the obtained steady state diffusivities represent values that are consistent with catalytic diffusivities (12–16) and usually are two to four orders of magnitude larger than uptake diffusivities. However, it is important to realize that the steady state diffusivities do not necessarily represent intrinsic self-diffusivities as determined by, for example, pulsed field gradient (PFG) nuclear magnetic resonance (NMR) studies. They describe net diffusivities based on the catalytic conditions applied, including its effects on transport phenomena as scaled to reaction kinetics for the zeolite (16, 17).

Fitting of the Uptake Curves

For crystals with slab geometry like mordenite, the experimental uptake curves may be described by the appropriate solution of Fick's second law (1, 18),

$$\frac{m_t}{m_{eq}} = 1 - \frac{8}{\pi^2}\sum_{n=0}^{\infty}\frac{1}{(2n+1)^2}\exp\left[-\frac{(2n+1)^2\pi^2 t D_{uptake}}{4L^2}\right], \qquad [4]$$

where m_t and m_{eq} represent the amounts of adsorption at time t and equilibrium, respectively, and L is the intracrystalline diffusion path length. If the experimental uptake curves are fitted using this equation, no good fits are obtained, as the time delay of the setup is not taken into account. The time delay occurs as a result of a concentration gradient over the catalyst bed, since no immediate constant concentration is established at the surface of the crystals after the start of the uptake experiment. The effect of this time delay on the experimental uptake curve may be approached by using the following relation (19)

$$C_t^{surface} = C_{eq}^{surface} * (1 - e^{-\beta \cdot t}), \qquad [5]$$

where β stands for a constant, which is equal to the reciprocal of the delay time.

The occurrence of intercrystalline diffusion in addition to intracrystalline diffusion and the presence of a stagnant layer around the zeolite particles may slow down the observed diffusion as well (1, 16, 17). However, based on check experiments shown in the results section of this paper (vide infra), it is argued that the uptake experiments will not suffer from a large influence of these phenomena, as convective gas transport predominates in the packed-bed reactor using a TEOM (Fig. 2).

The analytical solution for the transient diffusion equation including the correction for the time delay has been

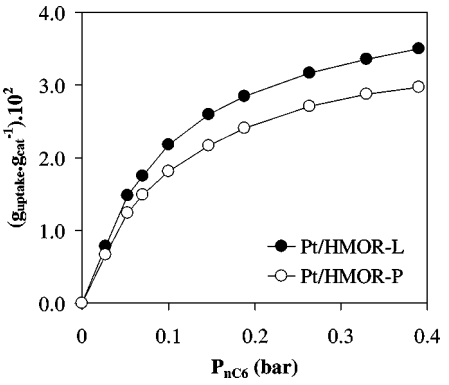

FIG. 2. Adsorption isotherms of *n*-hexane in Pt/HMOR-P and Pt/HMOR-L (in Table 2, experiments 2 and 7, respectively) determined under transient conditions at 523 K and a total pressure of 1.3 bar.

derived and reads

$$\frac{m_t}{m_{eq}} = \int_0^t \left\{ [1-\exp[-\beta(t-t')]] \sqrt{\frac{D_{uptake}}{\pi L^2 t'}} \sum_{n=0}^{\infty} \times \left[\exp\left[-\frac{L^2}{t' D_{uptake}} (2n+2)^2 \right] + \exp\left[-\frac{L^2}{t' D_{uptake}} (2n)^2 \right] - 2\exp\left[-\frac{L^2}{t' D_{uptake}} (2n+1)^2 \right] \right] \right\} dt'. \quad [6]$$

Mathematical information concerning the derivation and application of this equation is available from the authors. The experimental uptake data were fitted using this equation and the best fits yielded the parameters L^2/D_{uptake} and β. To determine D_{uptake} the intracrystalline diffusion path length L must be known. The obtained uptake diffusivity can be transformed into a steady state diffusivity (D_{ss}) by applying Eq. [3].

Thiele Modulus and Rate Constants

The extent to which diffusional transport limits the reaction rate can be quantified using the Thiele relationship giving the effectiveness of a catalyst (η) as a function of the dimensionless Thiele modulus (ϕ):

$$\eta = \frac{\tanh \phi}{\phi}. \quad [7]$$

When the Thiele modulus is small, the effectiveness factor approaches unity; this means there is very little variation in reactant concentration through the zeolite crystal and the rate of the reaction is controlled by the intrinsic chemical kinetics. On the other hand, when the Thiele modulus is large, the reactant concentration will become significantly lower, going from the outside to the inside of the zeolite crystal, and the reaction is said to be diffusion controlled or diffusion limited (1). To obtain the Thiele modulus, one first has to determine the apparent reaction rate constant. As the hydroisomerization reaction is approximately first order in *n*-hexane (20), the volumetric first-order rate constant based on the micropore volume may be calculated using

$$k_v^{\text{apparent}} = -\frac{\phi_v}{V_{micropores}} \ln(1-X), \quad [8]$$

where k_v is the volumetric rate coefficient (s^{-1}), ϕ_v is the total volumetric flow of feed at actual conditions ($m^3\,s^{-1}$), $V_{micropores}$ is the total micropore volume of the catalyst crystals (m^3), and X is the conversion of *n*-hexane. The Thiele modulus can then be computed using

$$\phi = L\sqrt{\frac{k_v}{D_{ss}}}. \quad [9]$$

Note that steady state diffusivities are used in this equation, as the Thiele model holds for k_v and D at identical concentration basis (13). From the Thiele modulus the effectiveness factor can be determined using Eq. [7]. The intrinsic rate coefficient is then computed using

$$k_v^{\text{intrinsic}} = \frac{k_v^{\text{apparent}}}{\eta}. \quad [10]$$

By filling out the obtained intrinsic rate constant in Eq. [9], subsequently followed by calculating Eqs. [7] and [10] again, a better approximation of the intrinsic rate coefficient is acquired. This process is repeated until no noticeable change in the obtained intrinsic rate constant is observed.

RESULTS

Uptake Experiments

The adsorption isotherms obtained at 523 K for *n*-hexane in Pt/HMOR-P and Pt/HMOR-L are depicted in Fig. 2. For Pt/HMOR-L the isotherm was found to be fully reversible; however, for Pt/HMOR-P it was not, most likely as a result of the formation of branched products that remain trapped inside the crystals.

The fitting results of all *n*-hexane uptake experiments are collected in Table 2, with the experiment number denoted in the first column. All experimental uptake curves were fitted using Eq. [6], so that values for the uptake diffusional time constant (L^2/D_{uptake}) and the parameter β are obtained. To calculate the uptake diffusion coefficient, the square of the intracrystalline diffusion path length L is divided by the uptake diffusional time constant (L^2/D_{uptake}). For HMOR-P, L is 0.2 μm, established from TEM data (9). For HMOR-L, L is estimated to be 0.06 μm by multiplying the ratio of the mesopore areas for HMOR-P and HMOR-L, determined by nitrogen physisorption (Table 1), with the L of HMOR-P. The steady state diffusivities are calculated

TABLE 2

Results of *n*-Hexane Uptake Experiments Performed on Pt/H–Mordenite Samples at 523 K and 1.3 bar

Experiment		Experimental conditions			Fitting results						
No.	Sample	Mass (mg)	Flow (ml min^{-1})	H_2/n-C_6 (mol mol^{-1})	L^2/D_{uptake} (s)	β^{-1} (s)	Chi^2[a]	L (m)	D_{uptake} (m^2 s^{-1})	C_{eq}/C_{gas}	D_{ss} (m^2 s^{-1})
1	HMOR-P	85	21.7	11	139	125	5×10^{-3}	2×10^{-7}	2.9×10^{-16}	328	1.0×10^{-13}
2	Pt/HMOR-P	85	21.7	11	147	109	7×10^{-3}	2×10^{-7}	2.7×10^{-16}	311	0.8×10^{-13}
3		85	20.9	22	161	99	8×10^{-3}	2×10^{-7}	2.5×10^{-16}	412	1.0×10^{-13}
4		85	43.4	11	158	58	9×10^{-3}	2×10^{-7}	2.5×10^{-16}	318	0.8×10^{-13}
5		17	21.7	11	154	21	6×10^{-3}	2×10^{-7}	2.6×10^{-16}	301	0.8×10^{-13}
6	HMOR-L	85	21.7	11	14	114	8×10^{-3}	6×10^{-8}	2.6×10^{-16}	409	1.1×10^{-13}
7	Pt/HMOR-L	85	21.7	11	16	104	6×10^{-3}	6×10^{-8}	2.2×10^{-16}	396	0.9×10^{-13}
8		85	20.9	22	19	88	6×10^{-3}	6×10^{-8}	1.9×10^{-16}	519	1.0×10^{-13}
9		85	43.4	11	20	61	8×10^{-3}	6×10^{-8}	1.8×10^{-16}	400	0.7×10^{-13}
10		17	21.7	11	21	25	9×10^{-3}	6×10^{-8}	1.7×10^{-16}	393	0.7×10^{-13}

[a] $\text{Chi}^2 = \sum_i (y_i^{obs} - y_i^{calc})^2$, where y is the uptake and i is the time parameter. (Note: $y_{max} = 1$.)

by multiplying the uptake diffusivity with the ratio of all sorbed species at equilibrium and the gas-phase concentration (12), according to Eq. [3].

In order to visualise the influence of the acid leaching treatment on the *n*-hexane uptake, the curves for Pt/HMOR-P and Pt/HMOR-L (in Table 2, experiments 2 and 7, respectively) are given in Fig. 3. The curves are measured at 0.1 bar *n*-hexane partial pressure, hence at the border of the linear part of the respective isotherm. From Fig. 3 it is obvious that the rate and amount of adsorption are significantly enlarged as a result of the acid treatment. In Fig. 4, the fits for these experiments are displayed and it is demonstrated that the Fickian diffusion model given in Eq. [6] is appropriate for describing the uptake curves obtained with our experimental setup. The linear behavior of the curves originates from the presence of the experimental time delay of the setup, described by Eq. [5], as earlier reported by Karge and Niessen (19). The presence of this time lag causes the absence of "square root" behavior in the experimental and fitted uptake curves. To check the validity of the application of a Fickian diffusion model, uptake curves have also been conducted at lower *n*-hexane partial pressure (i.e., within the linear part of the isotherm). Experiments 3 and 8 in Table 2 represent the measurements performed at this lower *n*-hexane partial pressure of 0.05 bar (H_2/nC_6 molar ratio of 22). Since values for the diffusivities obtained under these conditions are similar to those obtained at 0.1 bar *n*-hexane partial pressure, it is inferred that a Fickian diffusion model, as represented in Eq. [6], is applicable to the evaluation of the uptake data obtained in this study.

To check whether the occurrence of intercrystalline diffusion may play a role in these experiments, *n*-hexane uptake curves were also measured with a doubled flow rate of both

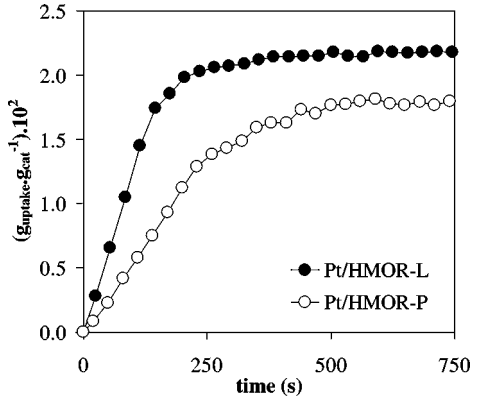

FIG. 3. Experimental uptake curves for *n*-hexane over Pt/HMOR-P and Pt/HMOR-L (in Table 2, experiments 2 and 7, respectively) using an 85-mg sample and a H_2/n-C_6 molar ratio of 11; *n*-hexane is introduced stepwise to the sample at time zero.

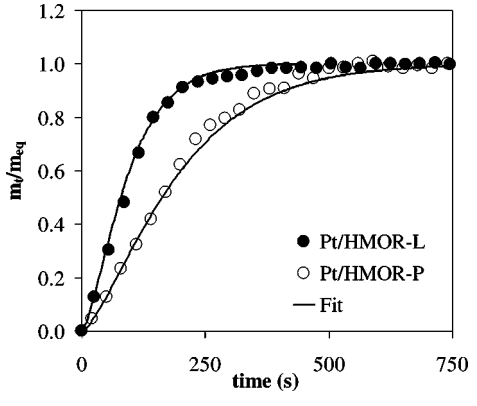

FIG. 4. Experimental (normalized) and fitted curves for *n*-hexane over Pt/HMOR-P and Pt/HMOR-L for the experiments conducted with an 85-mg sample and a H_2/n-C_6 molar ratio of 11 (fits are obtained using Eq. [6]).

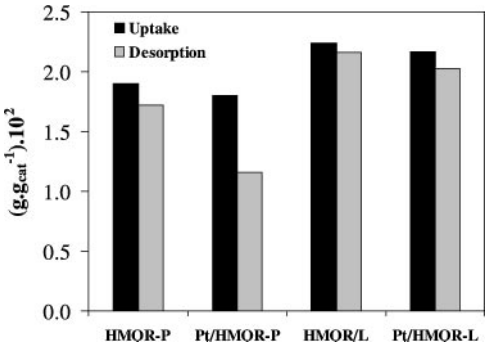

FIG. 5. Amounts of uptake (adsorption) and desorption for HMOR-P, Pt/HMOR-P, HMOR-L, and Pt/HMOR-L at 523 K and a H_2/*n*-C_6 molar ratio of 11.

n-hexane and H_2, and with a five times lower amount of catalyst as shown in Table 2 experiments 4, 9 and 5, 10, respectively. From this it is clear that the parameter β^{-1} proportionally decreases with a doubling of the feed or a lowering of the amount of catalyst while the same values for L^2/D_{uptake} were obtained.

By studying samples without platinum, the influence of product formation on the uptake of *n*-hexane was checked. Since similar values of L^2/D_{uptake} for both HMOR-L and Pt/HMOR-L (experiments 6 and 7) and for HMOR-P and Pt/HMOR-P (experiments 1 and 2) were obtained, it is concluded that the uptake measurements performed do not suffer from counterdiffusion between reactant and product molecules.

From Table 2 it is clear that after acid leaching, a decrease in diffusional time constants (L^2/D_{uptake}) is observed (i.e., the times to reach an equilibrium amount of uptake in the crystals is shorter). However, after taking into account the estimated diffusion path lengths and applying Eq. [3], both samples display steady state diffusivities (D_{ss}) in the same order of magnitude. This implies that the enhanced uptake after acid leaching is predominantly due to a decreased diffusion path length L.

The total amounts of molecules that desorb following the uptake experiments have been determined for HMOR-P, Pt/HMOR-P, HMOR-L, and Pt/HMOR-L and are displayed in Fig. 5. The reduced desorption of molecules for Pt/HMOR-P as compared to HMOR-P, HMOR-L, and Pt/HMOR-L is clearly illustrated and most likely arises from the formation of branched products which remain trapped as immobile species inside the parent mordenite crystals.

TABLE 3

Results for *n*-Hexane Hydroisomerization at 523 K, 1.3 bar, and H_2/*n*-C_6 = 11 mol mol^{-1}

Sample	Pt/HMOR-P	Pt/HMOR-L
Flow (ml min^{-1})	21.7	43.4
Sample amount (mg)	17	6
Conversion (mol%)	3.9	3.0
Relative activity	1	4.2
Selectivity to monobranched	0.78	0.82
Selectivity to dibranched	0.02	0.01
Selectivity to cracking products	0.20	0.17

TABLE 4

Rate Constants and Thiele Modulus Determined Using Eqs. [7]–[10]

Sample	T (K)	$k_{apparent}$ (s^{-1})	ϕ	η	$k_{intrinsic}$ (s^{-1})
Pt/HMOR-P	523	4.5	2.3	0.42	10.7
Pt/HMOR-L	523	18.7	1.0	0.77	24.2

Catalytic Testing

In Table 3 the *n*-hexane hydroisomerization activities and product selectivities for Pt/HMOR-P and Pt/HMOR-L at 523 K are collected. Results are obtained under differential conditions (3–4% conversion) by varying the flow rate and amount of catalyst. After acid leaching the relative activity per gram increases, confirming the results of Tromp *et al.* (9) and others (3, 4, 7). Both samples show high selectivities to monobranched isomers, although dibranched isomers and cracking products were also formed. The acid leaching resulted in a slight increase in the selectivity to monobranched products, while the selectivities toward dibranched and cracking products decreased. This is in agreement with results from Chica and Corma (21).

Based on the experimentally applied conditions and the differentially measured conversions, the Thiele modulus, effectiveness factor, and apparent and intrinsic rate constants are calculated for both Pt/HMOR-P and Pt/HMOR-L at 523 K using Eqs. [7]–[10]. Both the effectiveness factor and intrinsic activity are about doubled after the acid treatment. All numerical values are collected in Table 4.

DISCUSSION

Diffusion

From the raw data in Fig. 3 it is clear that the uptake of *n*-hexane is much faster in Pt/HMOR-L than in Pt/HMOR-P, indicating a higher accessibility as a result of the acid treatment. Fitting of the experimental data reveals the values for the diffusional time constant, L^2/D_{uptake}, and the time delay parameter β^{-1}, as displayed in Table 2. To test whether irregularities like the occurrence of intercrystalline diffusivity appear during the uptake measurements, check experiments have been performed, and as expected, β^{-1} proportionally decreased with a doubling of the feed or a lowering of the amount of catalyst while the same values for

L^2/D_{uptake} were obtained. Under the standard conditions applied here (85-mg sample, flow rate of 21.7 ml min^{-1}), the values for β^{-1} are around 100 s, illustrating the time delay of the setup. Based on the experimental conditions applied, the calculated minimum time to feed the required amount of *n*-hexane to a sample bed of 85 mg and establish a constant surface concentration should range from 10 to 40 s. The origin of the higher β^{-1} values observed results from the fact that in practice not all molecules in the feed stream adsorb in the uptake experiment. The experimental time delay causes the absence of square root behavior in the experimental and fitted uptake curves.

The fitting results demonstrate that the faster uptake of *n*-hexane for Pt/HMOR-L results in lower values for the diffusional time constants under all conditions applied. Dividing the square of the intracrystalline diffusion path length L by the uptake diffusional time constant (L^2/D_{uptake}) provides an estimate of the uptake diffusion coefficients. For Pt/HMOR-P, $L = 0.2$ μm, derived from TEM data (9). For Pt/HMOR-L, L is not exactly known, as by the acid treatment mesopores have been created, resulting in a less-ordered crystal structure. Nevertheless, based on nitrogen physisorption data the best estimate for the L of Pt/HMOR-L is 0.06 μm. This value seems to be reasonable when compared with a recently published 3D TEM study in which the mesopores of Pt/HMOR-L were visualized (10).

The steady state diffusivities are calculated by multiplying the uptake diffusivities with the ratio between the adsorbed species at equilibrium and the gas-phase concentration (Eq. [3]). This ratio is applied to allow integration of the uptake results with the simultaneously monitored catalytic properties of the Pt/H–mordenites. As is clear from Table 2, steady state diffusivities are in general two to three orders of magnitude larger than uptake diffusivities. This is consistent with diffusion data available on zeolites other than mordenite (12, 13, 15, 16).

It has been shown in the literature that acid leaching may result in the destruction of the mordenite crystals, accompanied by the formation of mesopores (22, 23). For the acid-leached sample (Pt/HMOR-L) we use in this study, this has been visualised by Tromp *et al.* (9) and Koster *et al.* (10). In addition, it has been shown that the acid treatment resulted in dealumination, the formation of extra framework aluminum, (i.e., Lewis acid sites), local destruction of the eight-membered ring side pockets, and/or the selective removal of acid sites (9). Despite the presence of all these phenomena, we observed no noticeable change in steady state diffusivities after acid leaching (Table 2), which indicates that the one-dimensional mordenite structure is still intact. This suggests that the accelerated uptake of *n*-hexane after acid leaching (i.e., the lower diffusional time constant (L^2/D_{uptake})) is predominantly caused by the shorter intracrystalline diffusion path length L resulting from the mesoporous structure of Pt/HMOR-L. The absolute values for the steady state diffusivities are low, as the numbers are based on the externally applied gas-phase concentration and may be affected by counterdiffusion effects, adsorption phenomena, and/or single-file diffusion (8, 24).

It has been suggested that the uptake of alkanes over Pt/H–mordenite proceeds in the single-file diffusion regime (3, 8), although there are conflicting data concerning this subject in the literature (25–27). In the case that this study could suffer from single-file diffusion, the Thiele model applied is no longer valid (24). However, mordenite is a 12-membered ring zeolite and the kinetic diameter of *n*-hexane is 4.3 Å. The occurrence of single-file diffusion is not likely at low prevailing *n*-hexane pressure (26). Moreover, counterdiffusion with product molecules is shown to have little influence, since similar values for D_{ss} are obtained for samples with (Pt/HMOR) and without platinum (HMOR). This leaves us with adsorption phenomena as the cause of the low values for D_{ss}. In other words, the concentration of mobile species in the pores is to all appearances (much) lower than the applied gas-phase concentration, meaning that the obtained steady state diffusivities do not necessarily represent the intrinsic self-diffusivities, as determined by, for example, PFG–NMR studies (17). However, several authors have stressed that values for steady state diffusivities coincide with the numbers for catalytically derived diffusivities (12–16), and therefore the values we have obtained in this study describe the net transport phenomena occurring in our Pt/H–mordenite samples under the catalytic conditions applied. To our knowledge, no PFG–NMR data on the diffusion of alkanes in mordenite are available in the literature, probably because of the inappropriate (too long) time scale for diffusion. In general, it must be stressed that differences in definitions of diffusivity can lead to different values of intracrystalline diffusivities and concentration dependencies (16). Considering the evaluation of results obtained by different groups, it is important that one specifies the conditions and methods under which diffusion experiments are executed.

Catalysis

As shown in Table 3, the *n*-hexane hydroisomerization activity per gram of catalyst is increased by a factor of 4.2 after acid treatment. This coincides with the higher accessibility of the Pt/HMOR-L (Fig. 3) that displays a mesoporous crystal structure (9, 10) with a higher amount of pore inlets available for reaction. During hydroisomerization, methylpentanes will be formed as primary products. For Pt/HMOR-P, the transport of branched products through the crystals will be more difficult, as the diffusion path length is longer, which results in the formation of secondary products. The reduced desorption of products for Pt/HMOR-P as compared to Pt/HMOR-L is further

illustrated in Fig. 5. Opening up the crystal structure on a mesoscopic scale, as is done by acid leaching, results in a faster exchange of reaction products and therefore a shift toward higher methylpentane selectivity and lower dimethylbutane selectivity, as summarized in Table 3. Under the conditions applied in this study, the activity of the Pt/H–mordenite catalysts will be affected by the intracrystalline transport, which implies that the accessibility of the active sites, and also their density and acidity, is of major importance. From the computed effectiveness factors (Table 4) it is clear that there is a large increase in the amount of catalyst that is effectively used after acid leaching. Moreover, from the intrinsic rate constants it is deduced that the intrinsic activity on a weight basis is doubled. Part of the increase as a result of the acid treatment therefore is explained by this increase in intrinsic activity, which is caused by an enhancement of the activity per Brønsted acid site resulting from the lower framework-aluminum content for Pt/HMOR-L. The other part of the increase in hydroisomerization activity is caused by an alleviation of intracrystalline diffusion limitation, which is predominantly induced by the shorter intracrystalline diffusion path length L resulting from the mesoporous structure that enables an enhanced transport of reactant and product molecules. The activity enhancement caused by acid leaching in this work is explained by roughly equal contributions from intrinsic activity and mass transport. The exact balance between the two, of course, will be sensitive to both details of the MOR-crystals and the reaction conditions in question.

CONCLUSIONS

Using a tapered element oscillating microbalance, it has been demonstrated for the first time that diffusivities can be established from uptake experiments performed under catalytic conditions. By applying an adapted diffusion model, uptake and steady state diffusivities for *n*-hexane in Pt/H–mordenite have been obtained. The diffusion of *n*-hexane in Pt/H–mordenite is not affected by counterdiffusion between reactant and product molecules. These quantitative results have been used for studying the effect of acid leaching on the performance of Pt/H–mordenite for *n*-hexane hydroisomerization.

Acid leaching largely accelerates the uptake and rate of hydroisomerization of *n*-hexane in Pt/H–mordenite, and in addition, an increase in primary reaction products is observed. An increase in the intrinsic activity and an alleviation of the intracrystalline diffusion limitation of hydrocarbon molecules equally cause the overall activity increase after acid leaching. The faster mass transfer is predominantly accounted for by a decrease in the intracrystalline diffusion path length resulting from the mesoporous structure created by acid leaching.

APPENDIX: NOTATION

C_{gas}, C_{eq}	gas phase concentration and adsorbed concentration at equlibrium [mol m^{-3}]
D_{uptake}, D_{ss}	uptake- and steady state diffusivity [m^2 s^{-1}]
f	frequency [s^{-1}]
k_v	volumetric rate coefficient [s^{-1}]
K_0	spring constant [g s^{-2}]
L	intracrystalline diffusion pathlength (= half length of crystal) [m]
m_t, m_{eq}	amount adsorbed at time t and equilibrium [g g_{cat}^{-1}]
m	mass [g]
t, t'	time and time integration parameter [s]
$V_{micropores}$	total micropore volume of the catalyst crystals [m^3]
x	distance [m]
X	conversion of *n*-hexane
β	delay constant [s^{-1}]
η	effectiveness factor
ϕ	Thiele modulus
ϕ_v	total volumetric flow of feed at actual conditions [m^3 s^{-1}]

ACKNOWLEDGMENTS

We thank M. Tromp, Utrecht University, for the start of this work and helpful discussions, and Dr. J. T. Miller, BP Amoco Research Center, Naperville, IL, for providing the samples. This work was financially supported by the Netherlands Organisation for Scientific Research (NWO, Project 700-97-019).

REFERENCES

1. Kärger, J., and Ruthven, D. M., "Diffusion in Zeolites and Other Microporous Materials." Wiley, New York, 1992.
2. Chen, D., Rebo, H. P., Moljord, K., and Holmen, A., *Chem. Eng. Sci.* **51**, 2687 (1996).
3. Lei, G. D., Carvill, B. T., and Sachtler, W. M. H., *Appl. Catal. A* **142**, 347 (1996).
4. Koradia, P. B., Kiovsky, J. R., and Asim, M. Y., *J. Catal.* **66**, 290 (1980).
5. Maxwell, I. E., and Stork, W. H. J., *in* "Introduction to Zeolite Science and Practice" (H. van Bekkum, E. M. Flanigen, and J. C. Jansen, Eds.), Vol. 38, p. 571. Elsevier Science, Amsterdam, 1991.
6. Sie, S. T., *in* "Advanced Zeolite Science and Applications" (J. C. Jansen, M. Stöcker, H. G. Karge, and J. Weitkamp, Eds.), p. 620. Elsevier Science, Amsterdam, 1994.
7. Corma, A., and Martinez, A., *in* "Catalytic Activation and Functionalisation of Light Alkanes: Advances and Challenges" (E. G. Derouane, J. Haber, F. Lemos, F. R. Ribeiro, and M. Guisnet, Eds.), p. 35. Kluwer Academic, Dordrecht, 1998.
8. Carvill, B. T., Lerner, B. A., Adelman, B. J., Tomczak, D. C., and Sachtler, W. M. H., *J. Catal.* **144**, 1 (1993).
9. Tromp, M., van Bokhoven, J. A., Garriga Oostenbrink, M. T., Bitter, J. H., de Jong, K. P., and Koningsberger, D. C., *J. Catal.* **190**, 209 (2000).
10. Koster, A. J., Ziese, U., Verkleij, A. J., Janssen, A. H., and de Jong, K. P., *J. Phys. Chem. B* **104**, 9368 (2000).

11. Zhu, W., van de Graaf, J. M., van den Broeke, L. J. P., Kapteijn, F., and Moulijn, J. A., *Ind. Eng. Chem. Res.* **37**, 1934 (1998).
12. Garcia, S. F., and Weisz, P. B., *J. Catal.* **121**, 294 (1990).
13. Post, M. F. M., *in* "Introduction to Zeolite Science and Practice" (H. van Bekkum, E. M. Flanigen, and J. C. Jansen, Eds.), Vol. 38, p. 391. Elsevier Science, Amsterdam, 1991.
14. Haag, W. O., Lago, R. M., and Weisz, P. B., *Faraday Discuss.* **72**, 317 (1982).
15. Garcia, S. F., and Weisz, P. B., *J. Catal.* **142**, 691 (1993).
16. Xiao, J., and Wei, J., *Chem. Eng. Sci.* **47**(5), 1143 (1992).
17. Bülow, M., and Micke, A., *Z. Phys. Chem.* **189**, 195 (1995).
18. Crank, J., "The Mathematics of Diffusion." Clarendon, Oxford, 1975.
19. Karge, H. G., and Niessen, W., *Catal. Today* **8**, 451 (1991).
20. Guisnet, M., Fouche, V., Belloum, M., Bournonville, J. P., and Travers, C., *Appl. Catal.* **71**, 295 (1991).
21. Chica, A., and Corma, A., *J. Catal.* **187**, 167 (1999).
22. Stach, H., Jänchen, J., Jerschkewitz, H. G., Lohse, U., Parlitz, B., Zibrowius, B., and Hunger, M., *J. Phys. Chem.* **96**, 8473 (1992).
23. Meima, G. R., *CATTECH* **2**(1), 5 (1998).
24. Kärger, J., Petzold, M., Pfeiffer, H., Ernst, S., and Weitkamp, J., *J. Catal.* **136**, 283 (1992).
25. van de Runstraat, A., van Grondelle, J., and van Santen, R. A., *J. Catal.* **167**, 460 (1997).
26. van de Runstraat, A., Kamp, J. A., Stobbelaar, P. J., van Grondelle, J., Krijnen, S., and van Santen, R. A., *J. Catal.* **171**, 77 (1997).
27. Rödenbeck, C., Kärger, J., Hahn, K., and Sachtler, W. M. H., *J. Catal.* **183**, 409 (1999).